Cu^+-specific CopB transporter: Revising P_{1B}-type ATPase classification

Rahul Purohit[a,b], Matthew O. Ross[a,b], Sharon Batelu[c], April Kusowski[c,d], Timothy L. Stemmler[c,d], Brian M. Hoffman[a,b], and Amy C. Rosenzweig[a,b,1]

[a]Department of Molecular Biosciences, Northwestern University, Evanston, IL 60208; [b]Department of Chemistry, Northwestern University, Evanston, IL 60208; [c]Department of Pharmaceutical Sciences, Wayne State University, Detroit, MI 48201; and [d]School of Medicine, Wayne State University, Detroit, MI 48201

Contributed by Amy C. Rosenzweig, January 12, 2018 (sent for review December 14, 2017; reviewed by Megan M. McEvoy and Gabriele Meloni)

The copper-transporting P_{1B}-ATPases, which play a key role in cellular copper homeostasis, have been divided traditionally into two subfamilies, the P_{1B-1}-ATPases or CopAs and the P_{1B-3}-ATPases or CopBs. CopAs selectively export Cu^+ whereas previous studies and bioinformatic analyses have suggested that CopBs are specific for Cu^{2+} export. Biochemical and spectroscopic characterization of *Sphaerobacter thermophilus* CopB (*St*CopB) show that, while it does bind Cu^{2+}, the binding site is not the prototypical P_{1B}-ATPase transmembrane site and does not involve sulfur coordination as proposed previously. Most important, *St*CopB exhibits metal-stimulated ATPase activity in response to Cu^+, but not Cu^{2+}, indicating that it is actually a Cu^+ transporter. X-ray absorption spectroscopic studies indicate that Cu^+ is coordinated by four sulfur ligands, likely derived from conserved cysteine and methionine residues. The histidine-rich N-terminal region of *St*CopB is required for maximal activity, but is inhibitory in the presence of divalent metal ions. Finally, reconsideration of the P_{1B}-ATPase classification scheme suggests that the P_{1B-1}- and P_{1B-3}-ATPase subfamilies both comprise Cu^+ transporters. These results are completely consistent with the known presence of only Cu^+ within the reducing environment of the cytoplasm, which should eliminate the need for a Cu^{2+} P_{1B}-ATPase.

P_{1B}-ATPase | copper homeostasis | copper efflux | CopB | CopA

Metal ions are required for critical cellular functions (1). In particular, copper is an essential cofactor in a multitude of proteins, but can be toxic, destroying iron–sulfur clusters and causing oxidative stress (2). Thus, regulating copper concentrations presents a major challenge to all organisms; 44% of the copper proteome has been assigned to copper homeostasis (3, 4). Proteins involved in copper homeostasis include metallosensors, metallochaperones, and membrane transporters (5). Among the transporters are the P_{1B}-ATPases, a subset of the P-type ATPase family (6). P_{1B}-ATPases are ubiquitous in nature and couple the energy of ATP hydrolysis to translocation of transition metal ions, including Cu^+, Cu^{2+}, Zn^{2+}/Cd^{2+}/Pb^{2+}, and Co^{2+} (7–9). P_{1B}-ATPases consist of six to eight transmembrane (TM) helices, an ATP-binding domain (ATPBD), an actuator domain, and in many cases, additional soluble metal-binding domains (MBDs), typically at the N terminus. Transport is accomplished via a classical Post-Albers cycle in which phosphorylation of a conserved aspartate residue in the ATPBD causes the enzyme to cycle between high (E1)- and low (E2)-affinity metal-binding states (10). In humans, defects in the Cu^+-transporting P_{1B}-ATPases ATP7A and ATP7B lead to Menkes syndrome and Wilson disease, respectively (11).

P_{1B}-ATPases have been categorized into seven subtypes (P_{1B-1}–P_{1B-7}) based on conserved motifs in the TM domain, the presence of different types of MBDs, and biochemical and genetic data linking individual transporters to specific metal ions (7, 12, 13). One of the key TM motifs is a three-residue, cysteine-containing sequence in TM helix 4; other conserved residues in TM helix 6 have also been considered in developing the classification scheme. Of the subclasses, the P_{1B-2}-ATPases transport Zn^{2+}, Cd^{2+}, and Pb^{2+} (CPC motif) (9, 14, 15), and the P_{1B-4}-ATPases transport Co^{2+}, Cd^{2+}, Zn^{2+}, and Fe^{2+} (SPC motif) (16–19). The metal specificities of the P_{1B-5} (PCP motif), P_{1B-6} (SCA motif), and P_{1B-7}-ATPases (CSC motif) remain unclear, although some evidence links the P_{1B-5}-ATPases to Ni^{2+} and Fe^{2+} (20, 21). The remaining two groups are the copper transporters. The P_{1B-1}-ATPases, which include ATP7A and ATP7B, transport Cu^+ (9, 22), whereas the P_{1B-3}-ATPases are proposed to transport Cu^{2+} (23, 24). These two subfamilies differ from one another in several ways. First, the TM helix 4 motif is CPC in the P_{1B-1}-ATPases and CPH in the P_{1B-3}-ATPases. The presence of this histidine has been widely assumed to confer a preference for Cu^{2+} (12, 13, 23, 24). The P_{1B-3}-ATPases, referred to as CopBs, are unique in that they contain a histidine-rich N-terminal extension that is proposed to be an MBD (23). This extension varies considerably in length, ranging from about 40–120 residues (*SI Appendix*, Fig. S1). By contrast, the P_{1B-1}-ATPases, of which many are designated CopAs, usually have MBDs comprising one to six ferredoxin-like domains characterized by a conserved CXXC metal-binding motif that binds a single Cu^+ ion (25).

The P_{1B-1}-ATPases have been studied intensively due to the link to Wilson and Menkes diseases (11), with multiple solution structures of the MBDs (25), electron microscopy structures of *Archaeoglobus fulgidus* CopA (26) and ATP7B (27), and a crystal structure of CopA from *Legionella pneumophila* (*Lp*CopA), albeit in the absence of bound copper or the MBD (28), available. In addition, the roles of the MBDs (29) and the nature of the TM Cu^+-binding site (9, 29) have been probed by a range of biochemical, biophysical, and functional studies. By contrast, just

Significance

Copper is an important biological cofactor, but can also be toxic in excess. Members of the P_{1B}-ATPase family of membrane transporters couple the energy of ATP hydrolysis to translocation of metal ions across membranes. P_{1B}-ATPases have been classified into groups on the basis of sequence and metal ion specificity. Two subfamilies, the P_{1B-1}-ATPases, which are linked to human diseases of copper metabolism, and the P_{1B-3}-ATPases, found only in bacteria, have been assigned as Cu^+ and Cu^{2+} transporters, respectively. Here we show that the P_{1B-3}-ATPases are actually Cu^+ transporters, necessitating revision of the classification scheme. These findings are consistent with the presence of only Cu^+ in the cytoplasm, which eliminates the need for a Cu^{2+} efflux pump.

Author contributions: R.P., M.O.R., T.L.S., B.M.H., and A.C.R. designed research; R.P., M.O.R., S.B., A.K., and T.L.S. performed research; R.P., M.O.R., S.B., A.K., T.L.S., B.M.H., and A.C.R. analyzed data; and R.P., M.O.R., T.L.S., B.M.H., and A.C.R. wrote the paper.

Reviewers: M.M.M., University of California, Los Angeles; and G.M., The University of Texas at Dallas.

The authors declare no conflict of interest.

[1]To whom correspondence should be addressed. Email: amyr@northwestern.edu.

This article contains supporting information online at www.pnas.org/lookup/suppl/doi:10.1073/pnas.1721783115/-/DCSupplemental.

Published online February 12, 2018.

a few studies of the P_{1B-3}-ATPases, which are found only in bacteria, have been reported. While early work on *Enterococcus hirae* CopB (*Eh*CopB) (30) suggested that it is a Cu^+ transporter, subsequent studies of thermophilic CopBs from *A. fulgidus* (*Af*CopB) (23) and *Thermus thermophilus* (*Tt*CopB) (31) indicated that CopBs are mainly Cu^{2+} transporters. Metal binding by the histidine-rich N-terminal region has not been investigated for any CopB. Thus, it remains unclear how the two classes of copper P_{1B}-ATPases confer selectivity for Cu^+ versus Cu^{2+}.

To investigate the basis for discrimination between Cu^+ and Cu^{2+} by P_{1B}-ATPases, we biochemically and spectroscopically characterized the CopB from *Sphaerobacter thermophilus* (*St*CopB), both with and without its 120-residue N-terminal histidine-rich domain. Contrary to prior reports and accepted dogma, our results indicate that *St*CopB is a Cu^+ transporter. Binding of Cu^{2+} is observed, but mutagenesis and electron paramagnetic resonance (EPR) spectroscopic data indicate that it is not located in the proposed TM binding site. Instead, X-ray absorption spectroscopic (XAS) studies on the Cu^+-bound protein define a sulfur-based coordination environment in the TM region. A reexamination of the bioinformatics analysis suggests that the P_{1B-1}- and P_{1B-3}-ATPases are subsets of the same class and provides a revised framework for overall P_{1B}-ATPase classification. Finally, insights into the possible role of the N-terminal histidine-rich region are presented.

Results and Discussion

StCopB Does Not Bind Cu^{2+} in the Archetypal P_{1B}-type ATPase TM Site. We initially assumed that *St*CopB is a Cu^{2+} transporter, as has been reported for *Af*CopB (23) and *Tt*CopB (31). To probe Cu^{2+} binding by the CopB TM metal-binding site and to investigate whether the N-terminal histidine-rich regions bind metal ions, we expressed and purified both full-length *St*CopB (WT-*St*CopB, residues 1–785) and *St*CopB lacking the N-terminal region (ΔMBD-*St*CopB, residues 114–785) (*SI Appendix*, Fig. S2). After overnight incubation with varying amounts of Cu^{2+}, followed by removal of excess copper, quantitation indicated that ΔMBD-*St*CopB binds a single Cu^{2+} ion even when incubated with a 10-fold excess (*SI Appendix*, Table S1). We first believed the Cu^{2+} to be bound at the TM-binding site reported in a recent study of *Af*CopB (24). Indeed, the EPR spectrum of ΔMBD-*St*CopB exhibited the type-2 Cu^{2+} signature (Fig. 1) reported for *Af*CopB ($g_{||}$ = 2.23, $g_{\perp}$ = 2.05, $A_{||}$ = 560 MHz for ΔMBD-*St*CopB; $g_{||}$ = 2.23, $g_{\perp}$ = 2.06, $A_{||}$ = 565 MHz for *Af*CopB) and attributed to nitrogen/oxygen (N/O) equatorial ligands on the basis of the Peisach–Blumberg correlation diagram (32). Consistent with this environment, electron-nuclear double resonance spectra collected on ΔMBD-*St*CopB identified at least one directly coordinated equatorial ^{14}N ligand and suggested the presence of a coordinated H_xO (*SI Appendix*, Fig. S3*A*).

Potential ligands to this presumed TM Cu^{2+}-binding site were identified by aligning a homology model of WT-*St*CopB (33) with the crystal structure of *Lp*CopA (28). In this model, the CPH motif of *St*CopB is in the same position as the CPC motif of *Lp*CopA (*SI Appendix*, Fig. S4). To assess whether the Cu^{2+}-binding site involves the CPH motif, as suggested for *Af*CopB (24), several variants (C404A, H406A, and C404A, H406A) of ΔMBD-*St*CopB were generated. Surprisingly, the EPR spectra of all three variants exhibited the same signal as ΔMBD-*St*CopB (*SI Appendix*, Fig. S3*B*), showing that the CPH motif is not the site of Cu^{2+} binding in *St*CopB.

We then investigated the Cu^{2+}-binding properties of full-length WT-*St*CopB. Reconstitution of WT-*St*CopB with increasing amounts of Cu^{2+} [0–15 equivalent (equiv)] indicated that it can bind up to approximately eight Cu^{2+} ions (*SI Appendix*, Fig. S5). Since ΔMBD-*St*CopB can bind approximately one Cu^{2+} ion, no fewer than seven Cu^{2+} ions must bind to the MBD. In fact, none of the spectra at loading concentrations between 0.75 and 10 Cu^{2+} equiv show the spectrum of ΔMBD-*St*CopB (*SI Appendix*, Fig. S3*C*). Instead, WT-*St*CopB loaded with 0.75 equiv Cu^{2+} exhibits a type-2 Cu^{2+} EPR signal ($g_{||}$ = 2.25, $g_{\perp}$ = 2.05, $A_{||}$ = 565 MHz) similar to, but distinct from, that of ΔMBD-*St*CopB, in particular with resolved ^{14}N hyperfine along $g_{\perp}$ (Fig. 1). The WT-*St*CopB spectrum shows a strong resemblance to that of Cu^{2+}-(imidazole)$_4$ (34). This similarity, combined with the abundance of histidine residues in the MBD, as well as the fact that this spectrum is distinct from that of ΔMBD-*St*CopB, suggests that histidine side chains in the MBD HXXH motifs (*SI Appendix*, Fig. S1) are the probable WT-*St*CopB Cu^{2+} ligands. Increasing the amount of Cu^{2+} increases the intensity of this signal without changing the Cu^{2+} $g_{||}$ and $A_{||}$ values, while the ^{14}N hyperfine splitting along $g_{\perp}$ is lost upon addition of 5 equiv Cu^{2+}. This observation indicates that the multiple Cu^{2+} sites in the MBD have very similar coordination spheres with similar sets of N/O ligands, but with slight variations in their imposed coordination geometries.

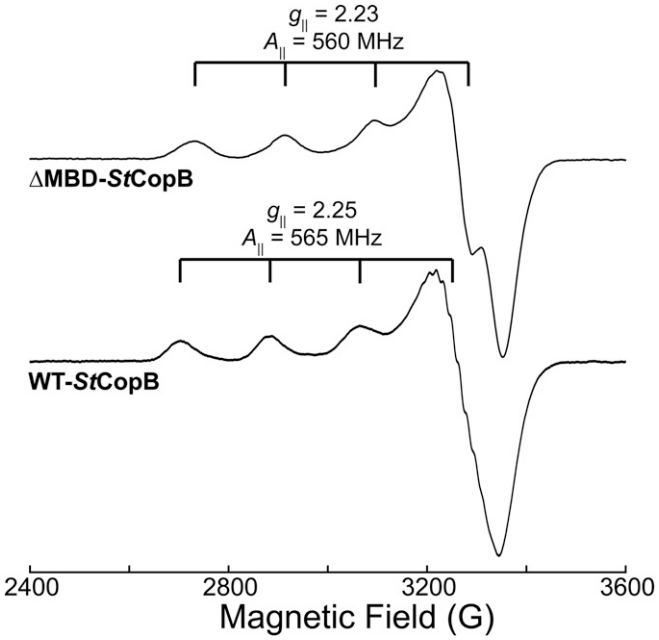

Fig. 1. EPR spectroscopic characterization of *St*CopB. Continuous wave (CW) X-band EPR spectra for (*Top*) ΔMBD-*St*CopB and (*Bottom*) 0.75 equiv Cu^{2+}-loaded WT-*St*CopB. Spectra were scaled to unity. Conditions: 9.36–9.37 GHz microwave frequency, 320 ms time constant, 16 G modulation amplitude, 80 s scan time, and 20 K temperature.

Diversity Among CopB MBDs and Characterization of the *St*CopB MBD. Sequence alignments show that CopB-MBD sequences are diverse in length and sequence (*SI Appendix*, Fig. S1). A close examination of these sequences reveals a strong resemblance to hydrophilins, proteins characterized by high glycine content (>6%) and a high hydrophilicity index (>1.0) (35). The *St*CopB-MBD sequence, which is composed of ∼27% histidine residues located in repeated HXXH and HXH motifs, has >13% glycine residues and is highly hydrophilic with a grand average of hydropathicity (36) score of −1.5. Polar ϕ-segments are present throughout the *St*CopB MBD, although the canonical hydrophilin (Y-, S-, and K-) segments (37) are largely absent, similar to the histidine-rich plant dehydrins, which are involved in protecting cells from a variety of stress conditions, particularly osmotic and toxic metal stress (38).

To probe metal binding by the isolated *St*CopB MBD, recombinantly expressed *St*CopB MBD (residues 1–120, without added histidine tag) was purified using a Ni-NTA column (*SI Appendix*, Fig. S2). Consistent with secondary and tertiary structure predictions (*SI Appendix*, Fig. S6), the circular dichroism (CD) spectrum

of *St*CopB MBD exhibits a large negative signal at 198 nm, indicative of random coil secondary structure (*SI Appendix*, Fig. S7). Addition of one equivalent of metal (Ni^{2+}, Cu^{2+}, Zn^{2+}, or Ag^{+}) did not produce any spectral changes. Further metal addition led to protein precipitation, reminiscent of the metal-induced aggregation reported for histidine-rich plant dehydrins (39). The CD spectrum collected in the presence of 33% 2,2,2-trifluoroethanol, known to stabilize secondary structure in proteins (40, 41), showed high helical content (208 and 222 nm), suggesting that *St*CopB MBD can form an ordered secondary structure (*SI Appendix*, Fig. S7). In addition, homology modeling of WT-*St*CopB predicts multiple different folds for the MBD within WT-*St*CopB, including a small ferredoxin-like fold or several helices (*SI Appendix*, Fig. S6). Thus, it might adopt a folded structure in the context of intact *St*CopB.

***St*CopB Is a Cu^{+}-Specific P_{1B}-ATPase.** We next measured the ATP hydrolysis activity of WT-*St*CopB and ΔMBD-*St*CopB in the presence of various divalent metal ions (Cu^{2+}, Ni^{2+}, Co^{2+}, or Zn^{2+}). The majority of previously characterized P_{1B-3}-ATPases, including *Af*CopB, *Tt*CopB, and a CopB from *Aquifex aeolicus* (*Aa*CtrA3), have been implicated in Cu^{2+} transport (23, 31, 42). Surprisingly, for both WT-*St*CopB and ΔMBD-*St*CopB, Cu^{2+}-dependent stimulation of ATPase activity was not observed (Fig. 2*A*). Moreover, the basal ATPase activity for WT-*St*CopB was inhibited at ≥10 μM Cu^{2+}, whereas Cu^{2+} addition did not affect the ΔMBD-*St*CopB basal activity. A similar effect was observed upon addition of Zn^{2+} to WT-*St*CopB and ΔMBD-*St*CopB (Fig. 2*A*). The observed inhibition could be due to binding of excess Cu^{2+} and Zn^{2+} by WT-*St*CopB (*SI Appendix*, Fig. S5). Conformational changes in the MBD might then hinder ATP hydrolysis by the ATPBD. WT-*St*CopB also exhibited some activity in the presence of Co^{2+}, but not in the presence of Ag^{+}, whereas ΔMBD-*St*CopB displayed the opposite trend with no activity stimulation by Co^{2+} and some activity upon Ag^{+} addition. Stimulation of ATPase activity and transport by Ag^{+} has been reported for *Af*CopB (23) and *Eh*CopB (30).

Since early studies of *Eh*CopB indicated that it is a Cu^{+} transporter (30), and since three other CopBs [*Af*CopB (23), *Tt*CopB (31), and *Aa*CtrA3 (42)] were in fact significantly active in the presence of Cu^{+} as well as Cu^{2+} (25, 50, and 50% of Cu^{2+}-stimulated activity, respectively), we considered the possibility that *St*CopB may be specific for Cu^{+} rather than Cu^{2+} and performed the ATPase activity assay in the presence of Cu^{+} generated by reduction of Cu^{2+} with 2-mercaptoethanol (2-ME). Unexpectedly, both WT-*St*CopB and ΔMBD-*St*CopB showed significant Cu^{+}-stimulated ATPase activity with maximal values of 123 ± 17 nmol P_i mg^{-1}·min^{-1} (basal activity: 42.5 ± 7.2 nmol P_i mg^{-1}·min^{-1}) and 50 ± 6 nmol P_i mg^{-1}·min^{-1} (basal activity: 18.8 ± 2.0 nmol P_i mg^{-1}·min^{-1}), respectively, at 55 °C, which is the optimal growth temperature for the bacteria (43) (Fig. 2*A*, *Inset*). Lipids (0.01% asolectin) were required to observe this metal-stimulated ATPase activity. The measured K_m values of 1.6 ± 0.3 μM and 2.5 ± 0.6 μM for Cu^{+} for WT-*St*CopB and ΔMBD-*St*CopB (Fig. 2*B*), respectively, are similar to previously reported K_m values for CopB and CopA (31, 44, 45). Furthermore, Cu^{+}-stimulated activity was eradicated by 1 mM bathocuproinedisulfonic acid (BCS) (Fig. 2*A*), a high-affinity Cu^{+}-specific chelator. The pronounced activity enhancement in the presence of Cu^{+} compared with all other metal ions tested indicates that *St*CopB is a Cu^{+}-specific transporter.

Having demonstrated that Cu^{2+} does not bind in the CPH TM site, we reasoned that this site might instead bind Cu^{+}. Consistent with this hypothesis, the three CPH motif variants (C404A, H406A, and C404A,H406A) did not exhibit Cu^{+}-stimulated ATPase activity (Fig. 2*C*). These results are at least in part due to disrupted binding of Cu^{+}. Whereas WT-*St*CopB and ΔMBD-*St*CopB bind ∼1 molar equiv of Cu^{+}, consistent with a single high-affinity Cu^{+}-binding site and no Cu^{+} binding by the MBD

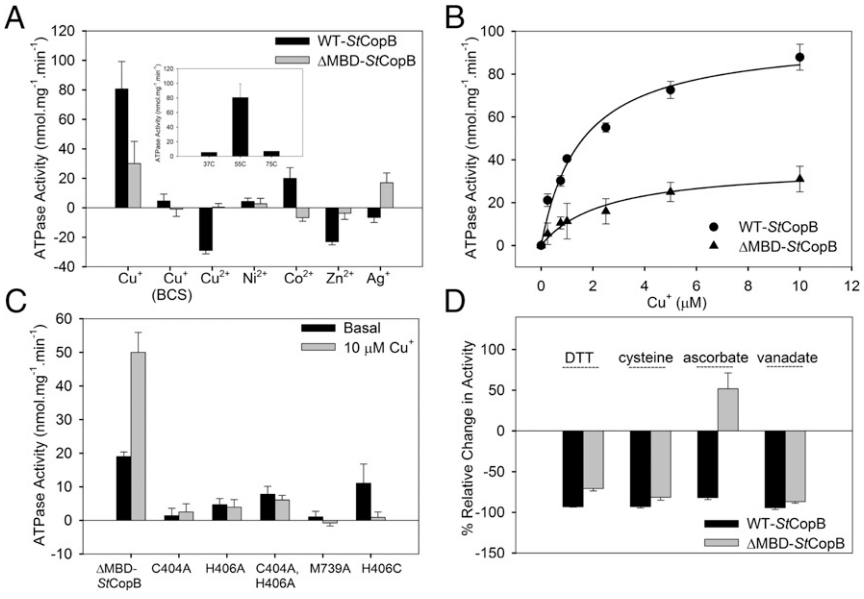

Fig. 2. Functional characterization of *St*CopB. (*A*) Metal-stimulated ATPase activity (nmol P_i mg^{-1}·min^{-1}) of WT-*St*CopB and ΔMBD-*St*CopB in the presence of 10 μM metal ions. Activity levels were corrected against basal activity in the absence of metal ions (WT-*St*CopB basal activity: 42.5 ± 7.2 nmol P_i mg^{-1}·min^{-1} and ΔMBD-*St*CopB basal activity: 18.8 ± 2.0 nmol P_i mg^{-1}·min^{-1}). The maximal ATPase activity was observed in the presence of 10 μM Cu^{+} (WT-*St*CopB: 123 ± 17 nmol P_i mg^{-1}·min^{-1}; ΔMBD-*St*CopB: 50 ± 6 nmol P_i mg^{-1}·min^{-1}). (*Inset*) Maximal Cu^{+}-stimulated WT-*St*CopB ATPase activity (basal corrected) at 37 °C, 55 °C, and 75 °C (representative values shown for 37 °C and 75 °C). (*B*) Specific ATPase activity (basal-corrected) of WT-*St*CopB (circles) and ΔMBD-*St*CopB (triangles) as a function of Cu^{+} concentration (μM) fitted to the equation $y = (V_{max} \times x)/(K_m + x)$. (*C*) Basal and Cu^{+}-stimulated ATPase activity levels of ΔMBD-*St*CopB and its variants. (*D*) Relative effects of various reducing agents (DTT, cysteine, ascorbate) on maximal Cu^{+}-stimulated ATP hydrolysis activity of WT-*St*CopB and ΔMBD-*St*CopB. Additionally, almost complete inhibition of ATPase activity was observed in the presence of 1 mM sodium orthovanadate, a phosphate analog and P-type ATPase competitive inhibitor. In all cases, error bars represent the SD of the average of at least three independent experiments.

(*SI Appendix*, Table S2), Cu^+ binding by ΔMBD-*St*CopB variants C404A, H406A, and C404A,H406A is diminished by ∼20–50%. Mutation of the conserved methionine in the TM helix 6 MSXST (12, 13) motif (M739A) also abolished activity, similar to what was observed for the *Lp*CopA M717V variant (46), although the M739A variant still bound close to 1 equiv of Cu^+. The lack of ATPase activity likely results from disruption of the ion release pathway as proposed for *Lp*CopA (46). Surprisingly, replacement of the conserved histidine residue in the CPH motif, H406, with cysteine to mimic the CPC motif in the Cu^+-transporting P_{1B-1}-ATPases resulted in similar basal ATPase activity to ΔMBD-*St*CopB, but absolutely no activity in the presence of Cu^+. However, this H406C variant can be reconstituted with ∼2.1 molar equiv of Cu^+ (*SI Appendix*, Table S2), suggesting that conversion of the CPH motif to a CPC motif introduces a second Cu^+-binding site.

To probe the apparent difference in metal selectivity between *Af*CopB and *St*CopB, we purified full-length *Af*CopB (residues 1–690) (*SI Appendix*, Fig. S2) and tested it for Cu^+-stimulated activity. Similar to what was reported by Meloni et al. (24), we observed no Cu^{2+}- or Cu^+-stimulated activity for purified *Af*CopB even in the presence of the lipids (0.01% asolectin). A V_{max} value of 1.2 μmol P_i $mg^{-1}{\cdot}h^{-1}$ (20 nmol P_i $mg^{-1}{\cdot}min^{-1}$) was reported for *Af*CopB in the presence of 1 μM $CuCl_2$, but may represent basal activity (24). We also tested *Af*CopB in *Escherichia coli* membranes prepared without any purification and detergent solubilization [similar to the procedure reported by Mana-Capelli et al. (23)] and observed very high basal activity at 75 °C with no detectable metal stimulation.

To further compare our results to previous work, we investigated the use of reductants other than 2-ME to generate Cu^+, specifically DTT and cysteine, which were used in other studies of CopAs (28, 44) and CopBs (24). In contrast to 2-ME, no Cu^+-stimulated ATPase activity for WT-*St*CopB or ΔMBD-*St*CopB was observed in the presence of DTT or cysteine (Fig. 2*D*). Similar levels of Cu^+-stimulated ATPase activity were obtained in the presence of ascorbate for ΔMBD-*St*CopB, but no stimulation was observed for WT-*St*CopB, which could be due to Cu^{2+}/ascorbate-mediated oxidation of the histidine residues in the MBD (47). It is important to note that DTT and cysteine can coordinate Cu^+, DTT with a $K_D \approx 10^{-15}$ M (48) and cysteine with a $K_D \approx 10^{-10}$ M (49). Formation of these high-affinity complexes limits the availability of Cu^+ and almost certainly accounts for the lack of Cu^+-stimulated ATPase activity using these reductants. Consistent with this notion, DTT and cysteine also inhibited the metal-stimulated activity of the P_{1B-4}-ATPase CzcP (18). We confirmed the complexation of Cu^+ by DTT and cysteine by monitoring Cu^+ chelation with BCS at ∼485 nm (*SI Appendix*, Fig. S8). Immediate Cu^+–BCS complex formation was observed upon addition of 2-ME or ascorbate, whereas reaction with DTT, cysteine, and tris(2-carboxyethyl)phosphine (TCEP) for 15 min failed to produce any significant Cu^+–BCS complex, indicating that Cu^+ is either sequestered by these reductants (DTT, cysteine) or not reduced (TCEP) and thus would not be available to stimulate ATPase activity. These findings explain the relative lack of Cu^+-stimulated activity observed for *Af*CopB (23) and *Tt*CopB (31), which were assayed in the presence of DTT. *Tt*CopB was in fact suggested to use Cu^+ in vivo (31).

A Sulfur-Containing Cu^+ Coordination Environment. To elucidate the atomic details of *St*CopB Cu^+ coordination within the TM region, we performed XAS analysis of Cu^+-loaded WT-*St*CopB. The WT-*St*CopB XANES spectrum exhibits a 1s→4p transition at 8,983 eV (Fig. 3*A*), consistent with the presence of Cu^+. Cu K-edge extended X-ray absorption fine structure (EXAFS) data of the Cu^+-loaded WT-*St*CopB (Fig. 3*B*) were best fit with a nearest-neighbor environment composed of three S ligands at an average bond length of 2.27 Å and one S ligand at 2.48 Å, with no long-range scattering observed (*SI Appendix*, Table S3). There

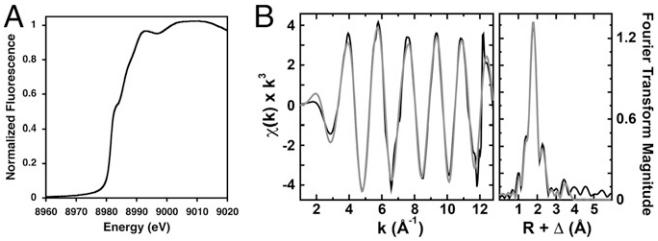

Fig. 3. X-ray absorption spectroscopic analysis of Cu^+-loaded WT-*St*CopB. (*A*) Normalized K-edge Cu XANES spectra of WT-*St*CopB. The peak at 8,984 eV corresponds to a Cu^+ 1s→4p transition. (*B*) Raw, unfiltered EXAFS data (black) and simulations (gray) (*Left*) and Fourier transforms of the raw EXAFS (black) and best-fit simulations (gray) (*Right*).

is no evidence for histidine coordination. Close inspection of the homology model and sequence alignment indicates the presence of a sulfur-lined inner channel that could be involved in Cu^+ transport (Fig. 4*A*). The EXAFS data suggest a TM Cu^+-binding site coordinated by Cys404 and potentially three methionine residues (Met186, Met187, Met224) in a tetrahedral fashion, although the presence of a chloride ligand cannot be ruled out. Similar sites involving Cu^+ coordinated by Cys and Met residues in a trigonal planar geometry have been proposed for *Lp*CopA (50) and human CTR1 (51). Importantly, all four proposed ligands are absolutely conserved among CopBs, with the methionine residues deriving from a PGMM motif in TM helix 1 and a MLLG motif in TM helix 2 (Fig. 4). These motifs, rather than the CopB CPH motif, likely confer metal specificity for Cu^+.

Comparison of CopB and CopA sequences indicates that many key residues proposed for Cu^+ transport by *Lp*CopA (50, 52) are highly conserved among CopBs as well (Fig. 4*B*). In particular, a channel lined with residues Met148, Met717, Glu189, Glu205, and Asp337 in *Lp*CopA corresponds to a proposed channel lined with Met186, Met739, Glu216, Glu231, and Asp362 in *St*CopB and is absolutely conserved among CopB and CopA sequences. In addition, *St*CopB Met224 is within the putative metal transport path and is strictly conserved among CopBs, but not in CopAs. This residue could potentially serve as a ligand in the absence of the second cysteine present in the CopA CPC motif, but not in the CopB CPH motif. The inhibitory effect of Cu^+ on the CPC *St*CopB mutant might therefore derive from Cu^+ binding in an incorrect conformation involving the second cysteine. These comparisons suggest that CopA and CopB utilize similar, but not identical, sets of residues to bind and export Cu^+.

Finally, we probed the copper coordination environment of Cu^{2+}-loaded ΔMBD-*St*CopB and the TM helix 4 CPH motif variants by XAS (*SI Appendix*, Fig. S9 and Table S4). Both the C404A and H406A variants displayed coordination environments similar to ΔMBD-*St*CopB, involving only N/O ligands and no S ligands. EXAFS fits with 3N/O and 1S ligands led to high Debye–Waller factors, indicating that an S ligand is not involved in Cu^{2+} binding. This result is in contrast to what was observed for *Af*CopB (24), but is consistent with the EPR analysis of these proteins (Fig. 1) as well as that of *Af*CopB (24). Additionally, the signature camelback feature observed in the Cu^{2+}-loaded ΔMBD-*St*CopB EXAFS indicates histidine ligation.

Revising the P_{1B}-ATPase Classification Scheme. Given the strong evidence that *St*CopB and likely the other characterized CopBs are actually Cu^+ transporters, we reexamined the classification of P_{1B}-ATPases into the P_{1B-1}–P_{1B-7} subfamilies (7, 12, 13). Notably, we identified several hundred P_{1B}-ATPase sequences that belong to a subgroup characterized by a conserved CPG motif in TM helix 4. No member of this P_{1B}-ATPase subfamily has been characterized. We then reinvestigated our previously generated

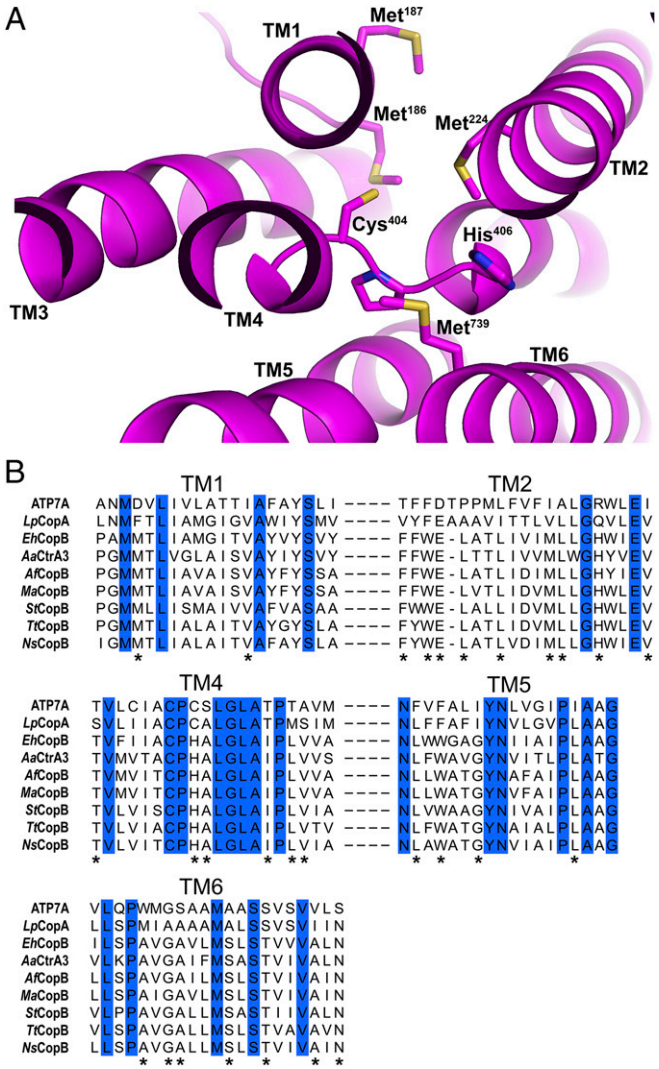

Fig. 4. Proposed *St*CopB Cu^+-binding site. (*A*) Close-up view of potential Cu^+-binding site in the *St*CopB homology model. Residues that may be important in Cu^+ binding and are absolutely conserved among CopBs include Met186 (TM1), Met187 (TM1), Met224 (TM2), and Cys404 (TM4). (*B*) Sequence alignment of the TM domains of human ATP7A, *L. pneumophila* CopA (*Lp*CopA), *E. hirae* CopB (*Eh*CopB), *A. aeolicus* copper transporter (*Aa*CtrA3), *A. fulgidus* CopB (*Af*CopB), *Methanosarcina acetivorans* CopB (*Ma*CopB), *S. thermophilus* CopB (*St*CopB), *T. thermophilus* CopB (*Tt*CopB), and *Nostoc* sp. CopB (*Ns*CopB) showing absolutely conserved residues (blue) among CopAs and CopBs. The residues absolutely conserved among CopBs are also highlighted (*).

P_{1B}-ATPase sequence similarity network (13), incorporating 250 of these CPG-containing sequences and 22 sequences containing the SCSC TM helix 4 motif (previously classified as P_{1B-7}-ATPases) into the clustering analysis (Fig. 5). Similar to the previous analysis, the sequences containing different TM helix 4 motifs clustered into distinct groups. The P_{1B-5} (PCP) and P_{1B-6} (SCA) subfamilies clustered separately, as previously observed. The CPG motif-containing sequences clustered strongly together, with some connections to the P_{1B-2} sequences containing the CPC motif. Importantly, the P_{1B-1} (CPC) and P_{1B-3} (CPH) subfamilies clustered separately as shown previously (13), but they are strongly connected when the network is visualized at 35% sequence identity, indicating that the two subfamilies are closely related. Moreover, they are more closely related to each other than both P_{1B-1} and P_{1B-2} sequences that contain the CPC motif. Finally, the SCSC motif-containing sequences clustered strongly within the P_{1B-2} subfamily, suggesting that these sequences are likely part of that subfamily rather than a separate subfamily.

Conclusions. The combined results indicate that *St*CopB is a Cu^+ transporter that binds a single Cu^+ ion in the TM region using four sulfur ligands. It does bind Cu^{2+}, but the mutagenesis data show that the TM Cu^{2+}-binding site does not involve the TM helix 4 CPH motif as hypothesized previously. Instead, EPR and EXAFS data indicate that Cu^{2+} is coordinated by N/O ligands, including histidine. The location of the Cu^{2+}-binding site remains unclear. The activity data clearly show that Cu^+, but not Cu^{2+}, stimulated ATP hydrolysis by *St*CopB, and previous reports of no Cu^+-stimulated activity can be attributed to the use of Cu^+-complexing agents as reductants. While the hydrophilin-like *St*CopB MBD is necessary for maximal activity, it surprisingly does not bind Cu^+. Instead, binding of approximately eight Cu^{2+} or Zn^{2+} ions inhibits basal ATPase activity, perhaps by interfering with the ATPBD. Thus, the MBD may have multiple functions, stabilizing the ATPBD during Cu^+ efflux and sequestering metal ions other than Cu^+ under conditions of stress, as observed in the similar plant dehydrins (38). The overall conservation of residues proposed to be important for copper transport by CopAs and CopBs is striking, and, taken together with the revised sequence similarity network, suggests that these two P_{1B}-ATPase subfamilies represent related solutions for Cu^+ transport rather than the existence of specific Cu^+ and Cu^{2+} transporters. This conclusion resolves a long-standing conundrum in the field: copper within the reducing environment of the cytoplasm should be Cu^+ (4, 31, 53, 54), obviating the need for a Cu^{2+} P_{1B}-ATPase.

Materials and Methods

Detailed procedures for preparation of *St*CopB proteins and variants, protein metal loading and quantitation, and ATPase activity assays are included in *SI Appendix, SI Materials and Methods*. Also described are computational methods for structure prediction, homology modeling, and sequence

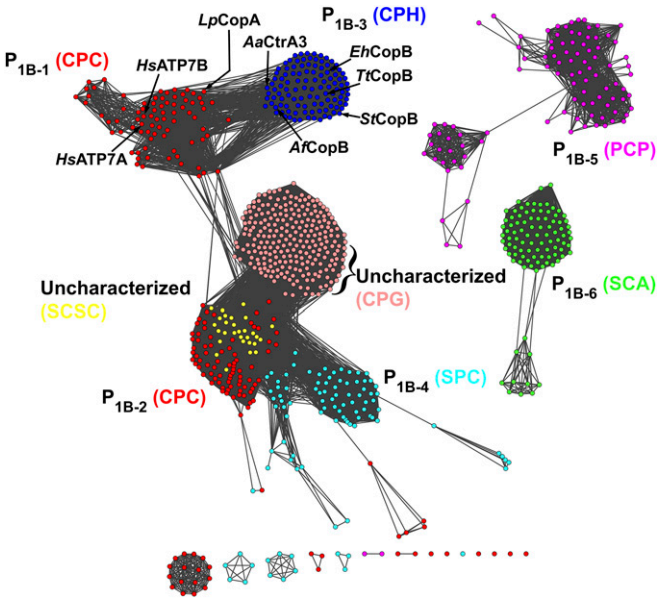

Fig. 5. The extended P_{1B}-ATPase similarity network. Sequences are represented as nodes (colored circles), and the strength of their similarity is indicated by edges (lines connecting colored circles). Sequences are color coded and labeled by their signature TM helix 4 motifs. The pink cluster represents newly identified sequences containing a conserved CPG motif. Representative CopAs and CopBs discussed in the text are labeled.

similarity network generation. Standard methods were used for collection of circular dichroism, EPR, and XAS spectroscopic data; instrument specifics are given in *SI Appendix, SI Materials and Methods*.

ACKNOWLEDGMENTS. This work was supported by National Institutes of Health (NIH) Grants GM58518 (to A.C.R.), GM118035 (to A.C.R.), DK068139 (to T.L.S.), GM111097 (to B.M.H.), and 5T32GM008382 (to M.O.R.). Portions of this research were carried out at the Stanford Synchrotron Radiation Lightsource (SSRL), a directorate of SLAC National Accelerator Laboratory and an Office of Science User Facility operated for the US Department of Energy Office of Science by Stanford University. The SSRL Structural Molecular Biology Program is supported by the Department of Energy Office of Biological and Environmental Research and by NIH–National Institute of General Medical Sciences (including Grant P41GM103393).

1. Waldron KJ, Rutherford JC, Ford D, Robinson NJ (2009) Metalloproteins and metal sensing. *Nature* 460:823–830.
2. Macomber L, Imlay JA (2009) The iron-sulfur clusters of dehydratases are primary intracellular targets of copper toxicity. *Proc Natl Acad Sci USA* 106:8344–8349.
3. Andreini C, Bertini I, Rosato A (2009) Metalloproteomes: A bioinformatic approach. *Acc Chem Res* 42:1471–1479.
4. Rensing C, McDevitt SF (2013) The copper metallome in prokaryotic cells: Metallomics and the cell, *Metal Ions in Life Sciences*, ed Banci L (Springer, Dordrecht, The Netherlands), Vol 12, pp 417–450.
5. Festa RA, Thiele DJ (2011) Copper: An essential metal in biology. *Curr Biol* 21: R877–R883.
6. Palmgren MG, Nissen P (2011) P-type ATPases. *Annu Rev Biophys* 40:243–266.
7. Argüello JM, Eren E, González-Guerrero M (2007) The structure and function of heavy metal transport P1B-ATPases. *Biometals* 20:233–248.
8. Argüello JM, González-Guerrero M, Raimunda D (2011) Bacterial transition metal P_{1B}-ATPases: Transport mechanism and roles in virulence. *Biochemistry* 50:9940–9949.
9. Sitsel O, et al. (2015) Structure and function of Cu(I)- and Zn(II)-ATPases. *Biochemistry* 54:5673–5683.
10. Albers RW (1967) Biochemical aspects of active transport. *Annu Rev Biochem* 36: 727–756.
11. Bull PC, Cox DW (1994) Wilson disease and Menkes disease: New handles on heavy-metal transport. *Trends Genet* 10:246–252.
12. Argüello JM (2003) Identification of ion-selectivity determinants in heavy-metal transport P_{1B}-type ATPases. *J Membr Biol* 195:93–108.
13. Smith AT, Smith KP, Rosenzweig AC (2014) Diversity of the metal-transporting P_{1B}-type ATPases. *J Biol Inorg Chem* 19:947–960.
14. Sharma R, Rensing C, Rosen BP, Mitra B (2000) The ATP hydrolytic activity of purified ZntA, a Pb(II)/Cd(II)/Zn(II)-translocating ATPase from *Escherichia coli*. *J Biol Chem* 275: 3873–3878.
15. Wang K, et al. (2014) Structure and mechanism of Zn^{2+}-transporting P-type ATPases. *Nature* 514:518–522.
16. Zielazinski EL, Cutsail GE, III, Hoffman BM, Stemmler TL, Rosenzweig AC (2012) Characterization of a cobalt-specific P_{1B}-ATPase. *Biochemistry* 51:7891–7900.
17. Raimunda D, Long JE, Padilla-Benavides T, Sassetti CM, Argüello JM (2014) Differential roles for the Co^{2+}/Ni^{2+} transporting ATPases, CtpD and CtpJ, in *Mycobacterium tuberculosis* virulence. *Mol Microbiol* 91:185–197.
18. Smith AT, Barupala D, Stemmler TL, Rosenzweig AC (2015) A new metal binding domain involved in cadmium, cobalt and zinc transport. *Nat Chem Biol* 11:678–684.
19. Patel SJ, et al. (2016) Fine-tuning of substrate affinity leads to alternative roles of *Mycobacterium tuberculosis* Fe^{2+}-ATPases. *J Biol Chem* 291:11529–11539.
20. Traverso ME, et al. (2010) Identification of a hemerythrin-like domain in a P_{1B}-type transport ATPase. *Biochemistry* 49:7060–7068.
21. Zielazinski EL, et al. (2013) *Sinorhizobium meliloti* Nia is a $P_{(1B-5)}$-ATPase expressed in the nodule during plant symbiosis and is involved in Ni and Fe transport. *Metallomics* 5:1614–1623.
22. Rosenzweig AC, Arguello JM (2012) Toward a molecular understanding of metal transport by P_{1B}-type ATPases: Metal transporters, *Current Topics in Membranes*, eds Lutsenko S, Argüello JM (Elsevier Academic Press, San Diego), Vol 69, pp 113–136.
23. Mana-Capelli S, Mandal AK, Argüello JM (2003) *Archaeoglobus fulgidus* CopB is a thermophilic Cu^{2+}-ATPase: Functional role of its histidine-rich-N-terminal metal binding domain. *J Biol Chem* 278:40534–40541.
24. Meloni G, Zhang L, Rees DC (2014) Transmembrane type-2-like Cu^{2+} site in the P_{1B-3}-type ATPase CopB: Implications for metal selectivity. *ACS Chem Biol* 9:116–121.
25. Boal AK, Rosenzweig AC (2009) Structural biology of copper trafficking. *Chem Rev* 109:4760–4779.
26. Allen GS, Wu CC, Cardozo T, Stokes DL (2011) The architecture of CopA from *Archaeoglobus fulgidus* studied by cryo-electron microscopy and computational docking. *Structure* 19:1219–1232.
27. Jayakanthan S, Braiterman LT, Hasan NM, Unger VM, Lutsenko S (2017) Human copper transporter ATP7B (Wilson disease protein) forms stable dimers in vitro and in cells. *J Biol Chem* 292:18760–18774.
28. Gourdon P, et al. (2011) Crystal structure of a copper-transporting PIB-type ATPase. *Nature* 475:59–64.
29. Lutsenko S, Gupta A, Burkhead JL, Zuzel V (2008) Cellular multitasking: The dual role of human Cu-ATPases in cofactor delivery and intracellular copper balance. *Arch Biochem Biophys* 476:22–32.
30. Solioz M, Odermatt A (1995) Copper and silver transport by CopB-ATPase in membrane vesicles of *Enterococcus hirae*. *J Biol Chem* 270:9217–9221.
31. Schurig-Briccio LA, Gennis RB (2012) Characterization of the P_{IB}-type ATPases present in *Thermus thermophilus*. *J Bacteriol* 194:4107–4113.
32. Peisach J, Blumberg WE (1974) Structural implications derived from the analysis of electron paramagnetic resonance spectra of natural and artificial copper proteins. *Arch Biochem Biophys* 165:691–708.
33. Wu CC, Rice WJ, Stokes DL (2008) Structure of a copper pump suggests a regulatory role for its metal-binding domain. *Structure* 16:976–985.
34. Silva KI, Michael BC, Geib SJ, Saxena S (2014) ESEEM analysis of multi-histidine Cu(II)-coordination in model complexes, peptides, and amyloid-β. *J Phys Chem B* 118: 8935–8944.
35. Battaglia M, Olvera-Carrillo Y, Garciarrubio A, Campos F, Covarrubias AA (2008) The enigmatic LEA proteins and other hydrophilins. *Plant Physiol* 148:6–24.
36. Kyte J, Doolittle RF (1982) A simple method for displaying the hydropathic character of a protein. *J Mol Biol* 157:105–132.
37. Rorat T (2006) Plant dehydrins–Tissue location, structure and function. *Cell Mol Biol Lett* 11:536–556.
38. Garay-Arroyo A, Colmenero-Flores JM, Garciarrubio A, Covarrubias AA (2000) Highly hydrophilic proteins in prokaryotes and eukaryotes are common during conditions of water deficit. *J Biol Chem* 275:5668–5674.
39. Mu P, et al. (2011) Cu^{2+} triggers reversible aggregation of a disordered His-rich dehydrin MpDhn12 from *Musa paradisiaca*. *J Biochem* 150:491–499.
40. Roccatano D, Colombo G, Fioroni M, Mark AE (2002) Mechanism by which 2,2,2-trifluoroethanol/water mixtures stabilize secondary-structure formation in peptides: A molecular dynamics study. *Proc Natl Acad Sci USA* 99:12179–12184.
41. Sönnichsen FD, Van Eyk JE, Hodges RS, Sykes BD (1992) Effect of trifluoroethanol on protein secondary structure: An NMR and CD study using a synthetic actin peptide. *Biochemistry* 31:8790–8798.
42. Chintalapati S, Al Kurdi R, van Scheltinga ACT, Kühlbrandt W (2008) Membrane structure of CtrA3, a copper-transporting P-type-ATPase from *Aquifex aeolicus*. *J Mol Biol* 378:581–595.
43. Pati A, et al. (2010) Complete genome sequence of *Sphaerobacter thermophilus* type strain (S 6022). *Stand Genomic Sci* 2:49–56.
44. Mandal AK, Cheung WD, Argüello JM (2002) Characterization of a thermophilic P-type Ag^{+}/Cu^{+}-ATPase from the extremophile *Archaeoglobus fulgidus*. *J Biol Chem* 277:7201–7208.
45. Solioz M, Stoyanov JV (2003) Copper homeostasis in *Enterococcus hirae*. *FEMS Microbiol Rev* 27:183–195.
46. Andersson M, et al. (2014) Copper-transporting P-type ATPases use a unique ion-release pathway. *Nat Struct Mol Biol* 21:43–48.
47. Requena JR, et al. (2001) Copper-catalyzed oxidation of the recombinant SHa(29-231) prion protein. *Proc Natl Acad Sci USA* 98:7170–7175.
48. Xiao Z, et al. (2011) Unification of the copper(I) binding affinities of the metallochaperones Atx1, Atox1, and related proteins: Detection probes and affinity standards. *J Biol Chem* 286:11047–11055.
49. Rigo A, et al. (2004) Interaction of copper with cysteine: Stability of cuprous complexes and catalytic role of cupric ions in anaerobic thiol oxidation. *J Inorg Biochem* 98:1495–1501.
50. Mattle D, et al. (2015) A sulfur-based transport pathway in Cu^{+}-ATPases. *EMBO Rep* 16:728–740.
51. De Feo CJ, Aller SG, Siluvai GS, Blackburn NJ, Unger VM (2009) Three-dimensional structure of the human copper transporter hCTR1. *Proc Natl Acad Sci USA* 106: 4237–4242.
52. Grønberg C, Sitsel O, Lindahl E, Gourdon P, Andersson M (2016) Membrane snchoring and ion-entry dynamics in P-type ATPase copper transport. *Biophys J* 111:2417–2429.
53. Foster AW, Osman D, Robinson NJ (2014) Metal preferences and metallation. *J Biol Chem* 289:28095–28103.
54. Cotruvo JA, Jr, Aron AT, Ramos-Torres KM, Chang CJ (2015) Synthetic fluorescent probes for studying copper in biological systems. *Chem Soc Rev* 44:4400–4414.